Chinese Journal of Chemical Engineering 55 (2023) 173–180

Contents lists available at ScienceDirect

Chinese Journal of Chemical Engineering

journal homepage: www.elsevier.com/locate/CJChE

Full Length Article

Molecular basis of cross-interactions between Aβ and Tau protofibrils probed by molecular simulations

Fufeng Liu [1,*], Luying Jiang [1], Jingcheng Sang [1], Fuping Lu [1], Li Li [2,*]

[1] State Key Laboratory of Food Nutrition and Safety, Key Laboratory of Industrial Fermentation Microbiology of Ministry of Education, Tianjin Key Laboratory of Industrial Microbiology, College of Biotechnology, Tianjin University of Science & Technology, Tianjin 300457, China
[2] College of Marine and Environmental Science, Tianjin University of Science & Technology, Tianjin 300457, China

ARTICLE INFO

Article history:
Received 7 February 2022
Received in revised form 18 April 2022
Accepted 26 April 2022
Available online 7 May 2022

Keywords:
Alzheimer's disease
Amyloid β-protein
Tau
Cross-interactions
Protein-protein docking
Molecular dynamics simulation

ABSTRACT

Amyloid β-protein (Aβ) and Tau, two common pathogenic proteins associated with Alzheimer's disease (AD), cross-interact, and thus co-assemble into hybrid aggregates. However, molecular mechanism of the cross-interactions remains unclear. To explore the issue, docking and molecular dynamics (MD) simulations were coupled to study the cross-interactions between Aβ pentamer and Tau pentamer. Four stable hybrid decamer conformations including double layer, single layer, block, and part-in were obtained by protein-protein docking software HADDOCK 2.2. Then, MD simulations were used to explore the molecular mechanism of cross-interactions between Aβ pentamer and Tau pentamer. The results of MD simulations showed that the part-in structure was the most stable among all the above four representative ones. The binding energy between Aβ and Tau was about −759.77 kJ·mol^{-1} in the part-in structure. Moreover, the part-in conformation would undergo conformational transition, which would improve its hydrophobicity and make the structure more compact. This work offers a structural understanding of cross-interactions between Aβ and Tau linked to AD.

1. Introduction

Occurrence and development of Alzheimer's disease (AD), one of the representative neurodegenerative diseases, are closely related to the misfolding and further aggregation of its pathogenic proteins [1,2]. Both extracellular amyloid plaques and intracellular neurofibrillary tangles are the two major pathologic markers of AD. Amyloid β-protein (Aβ) and Tau are the major constituents of amyloid plaques and neurofibrillary tangles, respectively. And the misfolding and aggregation of Aβ and Tau is considered the main causes for the formation of amyloid plaques and fibrous tangles, respectively. The amino acid sequence length of Aβ ranges from 36 to 43, and $Aβ_{42}$ and $Aβ_{40}$ are the two most common and abundant ones. Although Tau is bigger than Aβ and contains about 352–441 amino acids, it has the strong aggregation properties like Aβ. The R2−R4 area of Tau most likely formed orderly β-sheet structure in human brain of AD patients [3–5]. Especially, six residues region ($_{275}$VQIINK$_{280}$ and $_{306}$VQIVYK$_{311}$) in R2 and R3 plays an important role in Tau fibrillogenesis.

Recently, many *in vivo* and *in vitro* studies have proven that many amyloid proteins cross-interacted each other [6–11]. There is growing evidence that the cross-seeding of different amyloid proteins would promote their self-assemble [12–14]. For example, clinical and epidemiological studies have identified the diagnosis of type 2 diabetes as a risk factor for the development of AD due to the cross-seeding between Aβ and human islet amyloid polypeptide [15,16]. In addition, it has been identified that Aβ co-aggregated with Tau, which plays a crucial role in the occurrence and development of AD [17–20]. Previous studies have found that fibrous tangles of Tau are often accompanied by the appearance of Aβ plaques. Therefore, it can be speculated that the two amyloid proteins may copolymerize synergistically or accelerate each other. For example, Aβ aggregates can promote Tau aggregation, thus enhancing Tau pathology [21] and exacerbating brain lesions of AD patients [22]. Moreover, Lewis *et al.* [23] have also reported that the introduction of Tau in the brain of Tg2576 transgenic mice also enhances Aβ fibrillogenesis.

Although many *in vitro* and *in vivo* studies have been conducted [24–26], the molecular mechanism of the interactions between Aβ and Tau and their influence on each other's aggregation remains unclear. For example, Yifat *et al.* [27] explored the cross-interactions between Aβ tetramer and Tau tetramer by molecular

* Corresponding authors. Fax: +86 22 60602298.
E-mail addresses: fufengliu@tust.edu.cn (F. Liu), lili_2016@tust.edu.cn (L. Li).

https://doi.org/10.1016/j.cjche.2022.04.021
1004-9541/

dynamic (MD) simulations. They found that Aβ and Tau tetramers tend to form a lower energy stable complex. And Miller *et al.* [28] studied the cross-interactions between Aβ and NAC region of α-synuclein. The complex conformation of Aβ and α-synuclein was first obtained by docking. Then, two single layer conformation and three double layer conformation were identified. However, there are still some problems in the cross-interactions between different amyloid protein oligomers. For example, some 3D structure of Tau, only a small fragment in the repeated regions that are easy to form the β-sheet structure, are often applied [27,29–31]. In addition, the way of artificial selection is usually performed to gain the complex of different amyloid protein [28,32].

Herein, protein-protein docking and MD simulation methods were coupled to explore the cross-interactions between Aβ and Tau in atomic detail. First, Aβ-Tau hybrid decamer was obtained using the protein-protein docking software HADDOCK 2.2. Then, the change of each secondary structure and the number of contacts of the hybrid decamer were analyzed based on the results of MD simulations. Further, the change of binding energy between Aβ-Tau hybrid decamer was also probed by molecular mechanics-Poisson Boltzmann surface area (MM-PBSA) method. Thereafter, the interactions between Aβ and Tau pentamer in different conformations was also investigated. Finally, the novel part-in conformation obtained by docking was studied in detail. These results have important implications for understanding the cross-seeding of Aβ-Tau oligomers and the development of subsequent inhibitors combat against AD.

2. Materials and Methods

2.1. Protein-protein molecular docking

Both 3D structures of $A\beta_{42}$ (PDB ID: 5OQV [33]) and $Tau_{306\text{-}378}$ (PDB ID: 5O3O [34]) pentamer were obtained from the Protein Data Bank (https://www.rcsb.org/). In order to obtain the hybrid decamer model of Aβ-Tau, the protein-protein docking software HADDOCK 2.2 [35] was used. During the process of the protein-protein docking, only Aβ/Tau pentamer could form the free movement within cut-off of 0.5 nm and the relative positions of all main chain atoms of amyloid protein were fixed. Moreover, nonpolar hydrogen atoms were ignored. The distribution of protons of side chain of histidine's residues in Aβ/Tau pentamer was calculated using H^{++} online site (https://biophysics.cs.vt.edu/index.php) [36–38] at the neutral environmental conditions.

One thousand typical conformations were obtained from the HADDOCK results, and then top of 200 conformations were selected based on semi-flexible docking of HADDOCK 2.2. During the explicit solvent optimization, the system temperature was first gradually heated from 100 K to 310 K. Then, 1250 samples were obtained at 310 K with the time step of 2 fs.

Cluster analysis was performed based on the obtained 200 Aβ-Tau hybrid decamers. The cluster analysis script of HADDOCK 2.2 software was used based on the root mean square deviation (RMSD). The algorithm developed by Daura *et al.* [39] was applied to classify the conformation into each cluster with the cut-off of 0.75 nm. Finally, the HADDOCK score was used to select the typical Aβ-Tau hybrid decamers.

2.2. Molecular dynamics simulation

The typical conformations of the Aβ/Tau hybrid decamer were further analyzed by MD simulations. GROMACS 5.1.4 [40] software was used to perform MD simulation together with CHARMM36 force field with CAMP correction [41]. First, an Aβ-Tau hybrid decamer was placed in the center of a cubic box. Periodic boundary condition was used to simulate an infinitely solution environment. The minimum distance Aβ-Tau hybrid decamer from the edge was set as 1.0 nm. Then, TIP4P water model was used to fill the simulation box. At the same time, counter ions were added at random positions to neutralize the simulation system. Detailed parameters of different systems are shown in Table S1 (Supplementary Material).

The energy minimization simulation was first performed for 50000 steps using the steepest descent method to eliminate unreasonable atom-atom contacts. Under the isothermal-isometric (NVT) ensemble, the leap-frog integral algorithm was then used to integrate the motion equation with a time step of 2 fs for 100 ps equilibrium dynamics simulation [42,43]. Maxwell distribution was used to generate random initial velocities for all atoms. The LINCS [44] algorithm is used to constrain all covalent bonds containing hydrogen atoms. Verlet was used to calculate van der Waals interactions. Both van der Waals (VDW) and electrostatic (ELE) interactions of short distance truncated smoothly at 1 nm. And the list of non-bonding atoms was updated every 10 steps. Dispersion correction is applied to the energy and pressure terms to account for the truncation of van der Waals interactions. The particle mesh Ewald [45] method with the grid size of 0.016 nm was used to calculate the long-range electrostatic interactions, and its intercept was defined as 1.2 nm. Moreover, under the isothermal-isostatic (NPT) ensemble, the Parrinello-Rahman and V-rescale methods were used to maintain the standard atmospheric pressure of 0.1 MPa and constant temperature of 310 K in the system, respectively [46]. And the time and the pressure coupling constant was set to 0.1 ps and 2.0 ps, respectively. Next, NPT simulation was also performed for 100 ps. Finally, the production MD simulation is performed for 50 ns. And the MD trajectories, speed, energy, and log file were saved once every 50 ps.

2.3. Analysis of MD simulations

MD trajectories were analyzed using the built-in tools and related programs in the GROMACS 5.1.4 package. The *gmx sasa* and *gmx hbond* commands were used to calculate solvent accessible surface area (SASA) [47] and the number of inter-molecular hydrogen bonds between Aβ and Tau pentamers. The *gmx mindist* command was selected to analyze the distance between hydrophobic residues of Aβ and Tau pentamers with an intercept of 0.35 nm, which is commonly used to represent the hydrophobic interactions [48]. Likewise, it was also used to calculate the number of atom-atom contacts between Aβ and Tau pentamers.

Dictionary secondary structure of proteins (DSSP) [49] plug-in was used to analyze the secondary structure and calculate the content of each secondary structure of all residues in Aβ and Tau pentamers. Visual molecular dynamics (VMD) 1.9.4 software [50] was used to analyze the trajectory of MD simulation and render the screenshots. Moreover, the binding free energy between Aβ and Tau pentamers in Aβ-Tau hybrid decamer was calculated using the g_mmpbsa plugin [51].

3. Results and Discussion

3.1. Four typical Aβ-Tau hybrid decamers were identified

HADDOCK software was first used to obtain the typical structure of Aβ-tau decamers. Based on the cutoff of RMSD 0.75 nm of Aβ-Tau hybrid decamer, all conformations were divided into nine clusters. Then, four typical structures including double layer, block, single layer and part-in were obtained. Table S2 lists the results of protein-protein docking including type of conformation, HADDOCK score, number of conformations, vdW and electrostatic energies,

and embedded surface area (BSA). From Table S2, four typical conformations including double layer, block, single layer and part-in were identified. And their representative snapshots were shown in Fig. S1 and selected in the following MD simulations. Similar single layer morphology of Aβ and Tau complies was observed by Miller *et al.* [27]. They only observed the single layer motif because that both $A\beta_{17-42}$ and Tau repeats consist of two β-strands connected by U-turn. That is, initial structure of Aβ and Tau aggregates plays an important role in their cross-seeding. Moreover, the most unfavorable structure, a double layer conformation with the highest score of 300, was also selected for following study. Table 1 lists the typical conformations and HADDOCK score of five conformations.

3.2. Secondary structure analysis of Aβ-Tau hybrid decamer

Previous studies have found that amyloid protein aggregates are characterized by β-sheet-rich structure in parallel or antiparallel arrangement [52–54]. To explore the effect of different binding modes on the secondary structure of the hybrid decamer, the content of secondary structures of Aβ-Tau hybrid decamer was first calculated in the last 10 ns (Fig. 1). There are four typical secondary structure including β-sheet, coil, β-bridge and turn in Aβ-Tau hybrid decamer. Fig. 1(a) shows the content of each secondary structure of A−E conformation. As expected, the content of β-sheet structure takes overwhelming majority of the five conformations, indicating that all of five typical structures maintained β-sheet structures. However, it should be noted that the content of β-sheet structure in different conformations has slight difference (Fig. 1(a)).

To analyze the effect of Aβ-Tau hybrid decamer with different binding modes on the content of β-sheet, β-sheet content of each Aβ/Tau pentamer in five hybrid decamers were calculated. And pure Aβ and Tau pentamers were also selected for the control groups (Fig. 1(b) and 1(c)). As can be seen from Fig. 1(b), the cross-interaction between Aβ and Tau pentamers has little impact on β-sheet content of Tau, indicating that the overall structure of Tau is less susceptible to the Aβ pentamer binding. However, it is worth noting that the content of β-sheet of Tau only decreases in the E conformation (double layer) compared with the isolated system. It suggests that the cross-interaction for E conformation can reduce the β-sheet content of Tau. However, there is an enormous influence on the content of β-sheet in Aβ of Aβ-Tau hybrid decamer (Fig. 1(c)). For example, the cross-interactions play an important role in enhancement of the content of β-sheet of Aβ in B (single layer) and C (double layer) conformations, but it has almost no effect on A (block) and D (part-in) conformations. Moreover, the cross-interactions reduce the content of β-sheet of Aβ in E (part-in) conformation.

3.3. Analysis of the contact number of Aβ-Tau hybrid decamer

To explore the affinity between Aβ and Tau pentamers in different conformations, the time evolution of atom-atom contact number between Aβ and Tau pentamers in five conformations was first calculated (Fig. 2). The number of contacts between Aβ and Tau pentamers in A conformation rapidly decreased, ranging from 180 dropped to 40. It implies that the binding of Aβ and Tau pentamers in A conformation (block) is weak, and the conformation is also unstable. Similar phenomenon was observed as for E conformation. In the E conformation, for example, the number of contacts between Aβ and Tau pentamers decreased gradually, ranging from 210 at the initial state of MD simulation to 120 at the end of the MD simulation.

However, in conformations B and C, the atomic contact number between Aβ and Tau pentamers keeps relatively stable. In the D conformation, the number of contacts between Aβ and Tau pentamers fluctuate sharply during the first 10 ns. And then stabilized to about 140 in the last 40 ns MD simulation, indicating that the D conformation was relatively stable during most of the simulation time. Notably, although the number of contacts between Aβ and Tau pentamers in the E conformation finally drops to 120, the contact number is still much higher than the 40 in the A conformation.

Table 1
The typical conformation, HADDOCK score and type of the representing composite conformation in the data analysis

Typical conformation	HADDOCK score	Type
A	175	Block
B	173	Single layer
C	104	Double layer
D	219	Part-in
E	300	Double layer

3.4. Analysis of binding energy of Aβ-Tau hybrid decamer

Based on the last 10 ns MD trajectories, the MM-PBSA method was applied to calculate the average binding energy between Aβ and Tau and the results are shown in Fig. 3. The binding energy between Aβ and Tau in the four conformations (*i.e.*, A−D) is less than 0, indicating that the binding energy between Aβ and Tau in the A—D conformation is favorable. Especially, D conformation has the lowest binding energy (−759.77 $kJ \cdot mol^{-1}$), implying that the binding energy between Aβ and Tau in the part-in conformation is the strongest one. As expected, the average binding energy between Aβ and Tau in the E conformation is 250.61 $kJ \cdot mol^{-1}$ (Fig. 3). It implies that there are unfavorable interactions between Aβ and Tau in the double layer conformation. That is, the double layer structure is very unstable.

To further examine the contribution of residues of Aβ and Tau in different conformations, the average binding energy between Aβ and Tau was decomposed into each residue. The binding energy between different residues of Aβ and Tau in A−E conformations were shown in Figs. S2–S6, respectively. For clarity, residues with minor contribution were ignored. Although each residue of Aβ plays an important role in cross-interactions with Tau, the region of V313-G355 of Tau contributes greatly. In conformation A, only residues D7, G9, and Y10 of Aβ and residues V331 and P332 of Tau contribute greatly to the cross-interactions between Aβ and Tau (Fig. S2). That is, the binding ability between Aβ and Tau in conformation A is relatively weak, implying that the conformation A is unstable. As for conformation B, the residues F4, D7, E11, V18, F20, E22, and I41 of Aβ and the residues C322, G335, Q336, and V337 of Tau were found to contribute greatly in the cross-interactions between Aβ and Tau. Interestingly, these residues of Aβ mainly are acidic and non-polar residues, while these residues of Tau mostly are weak polar and non-polar residues (Fig. S3). Similar with conformation A, only 4 hot spots (*i.e.*, D7, S8, G9, and Y10) of Aβ and 2 residues (*i.e.*, N327 and I328) of Tau were identified in the conformation C (Fig. S4).

Fig. S5 shows the free energy decomposition of Aβ and Tau in the conformation D. The residues E3, D7, L34, M35 and V36 of Aβ and the residues L325, V331, R349 and G355 of Tau were identified. Especially, the negative charged residues E3 and D7 of Aβ and the positive charged residue R349 in Tau contributed greatly in the cross-interactions between Aβ and Tau. However, the positive charged residue R5 is unfavorable for the binding between Aβ and Tau. In addition to these charged residues, many hydrophobic residues including L34, M35, V36, L325, V331 also offer the favorable binding energy. Although the contribution of each

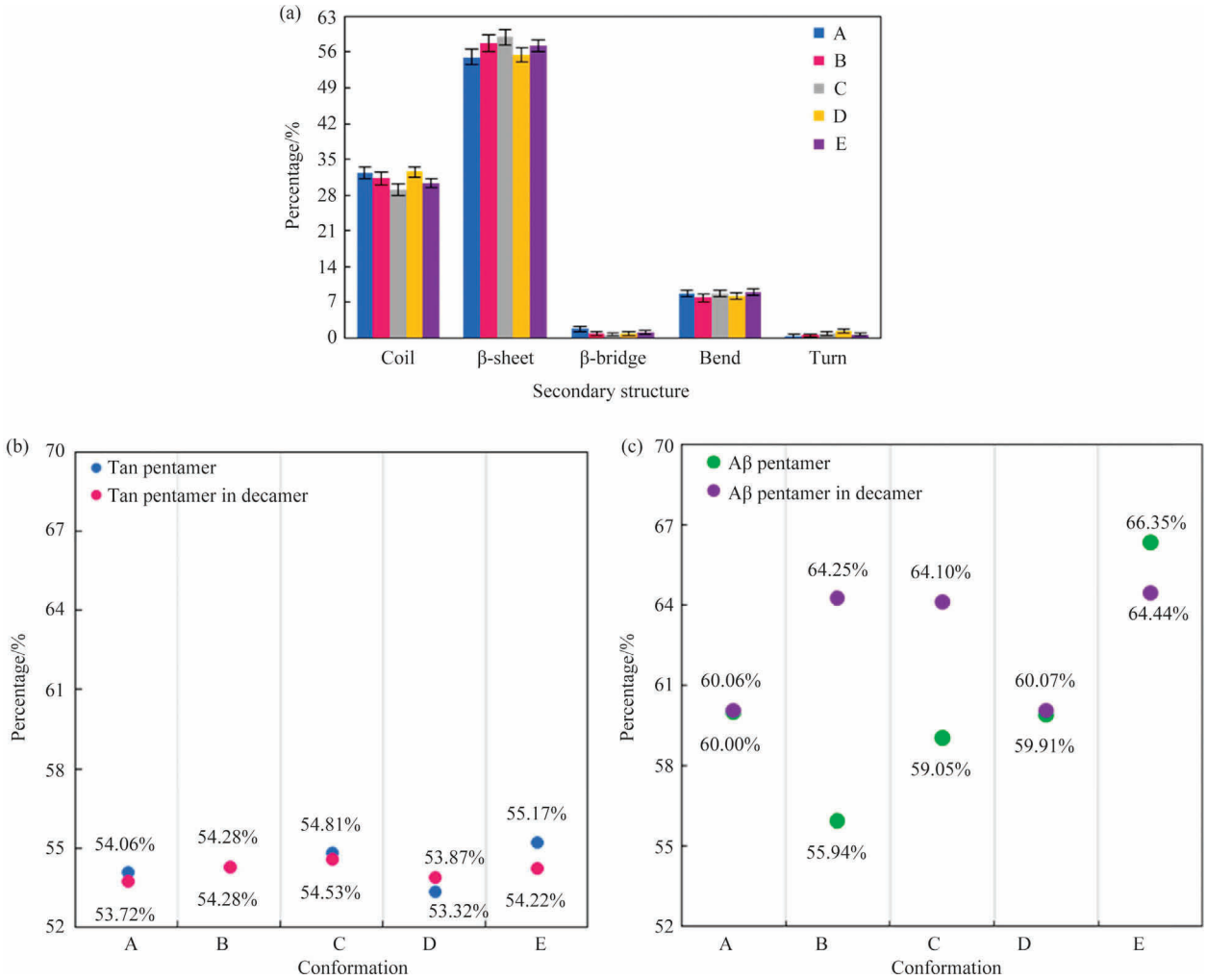

Fig. 1. (a) Average contents of each secondary structure including coil, β-sheet, β-bridge, bend and turn. Percentages of β-sheet structure in (b) Tau and (c) Aβ pentamers for conformations A–E in the last 10 ns MD simulation.

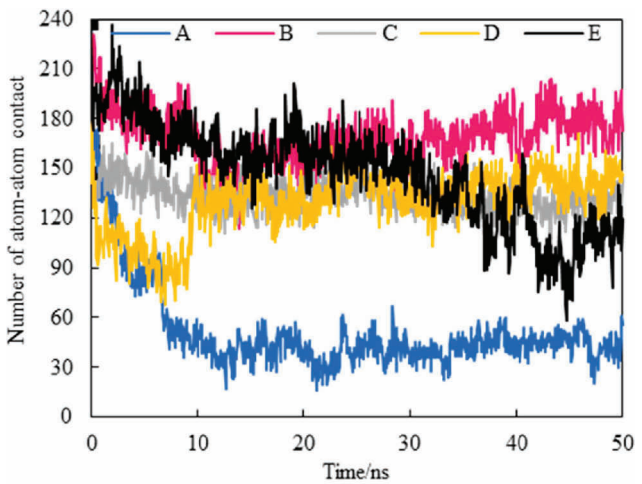

Fig. 2. The number of atom-atom contacts between Aβ pentamer and Tau pentamer in the conformations A–E as a function of simulation time.

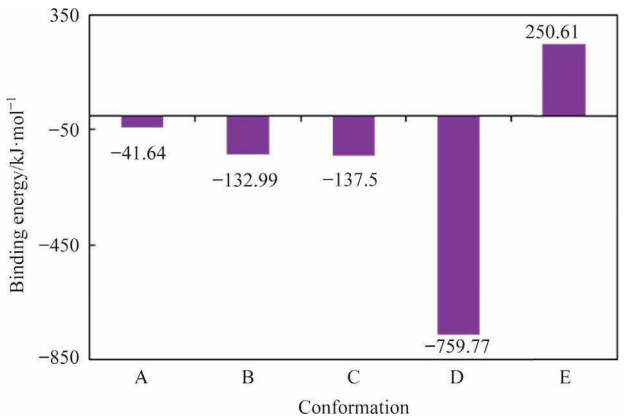

Fig. 3. Binding energy between Aβ pentamer and Tau pentamer for the conformations A–E based on the trajectories of last 10 ns MD simulation.

hydrophobic residue is low, the number of residues is tremendous. Thus, these hydrophobic residues still provide considerable non-polar binding energy.

In conformation E, the hydrophobic residues V331 and Q336 and negative charged residue E338 of Tau contributed greatly to the cross-interactions between Aβ and Tau (Fig. S6). In contrast, the positive charged residues of K16 and K340 offered positive energy. For example, the positive charged residue K16 of Aβ

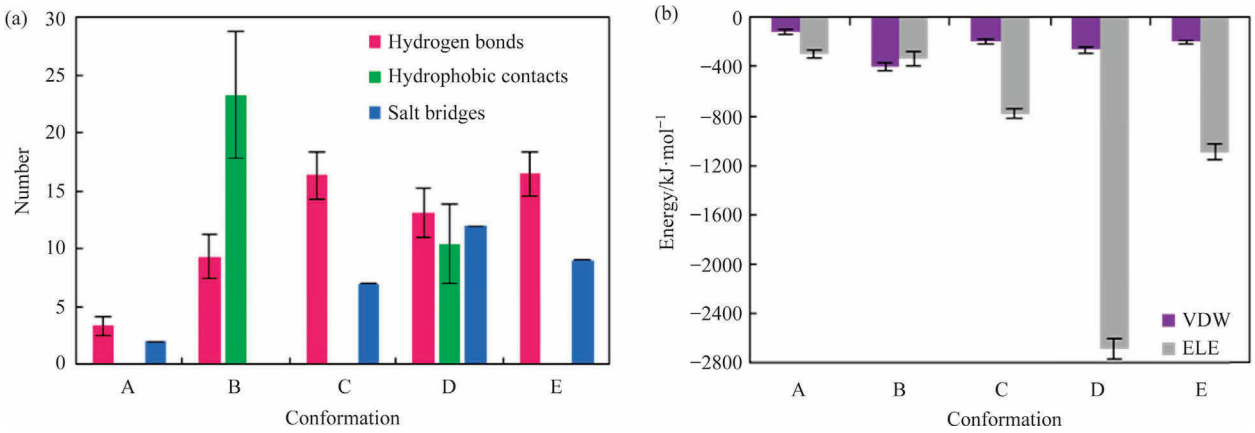

Fig. 4. (a) The types and quantities of non-bonding interactions and (b) the values of van der Waals binding energy and electrostatic binding energy between Aβ and Tau pentamers in the conformations A–E during the last 10 ns MD simulation.

contributed up to 75.3 kJ·mol^{-1}, implying that the residue K16 is unfavorable for the cross-interaction between Aβ and Tau.

3.5. Direct interaction and binding energy among Aβ-Tau hybrid decamer

Previous studies have proven that both hydrogen bonding and hydrophobic interactions play an important role in the formation and stabilization of Aβ fibrils and Tau proteins [55]. Herein, the direct interactions among five different Aβ-Tau decamers were first explored. During the last 10 ns, the common three kinds of direct interactions including hydrogen bonds, salt bridges and hydrophobic interactions were calculated and shown in Fig. 4(a). From Fig. 4(a), hydrogen bonds exist in all of five conformations. However, both salt bridges and hydrophobic interactions only exist in specific conformations. For example, hydrophobic interactions and salt bridges only occurred in the conformations B and D and C–E, respectively.

Fig. 4(b) shows the van der Waals (VDW) and electrostatic energies (ELE) of five conformations during the last 10 ns. As shown in Fig. 4(b), the values of electrostatic force are higher than that of van der Waals force for almost all conformations. Compared with other four conformations, the values of van der Waals and electrostatic interactions in conformation A are the lowest. Moreover, as for the conformations A, C, D and E, it should be noted that the electrostatic energy is stronger than that of VDW one. Especially for the conformation D, the electrostatic energy between Aβ and Tau is as high as −2700 kJ·mol^{-1}.

3.6. Comprehensive analysis of part-in conformation

The part-in conformation is a novel binding mode, which has not been studied yet. Moreover, the binding ability between Aβ and Tau in part-in conformation is the strongest, and thus their structure is also very stable. Therefore, a comprehensive analysis on the properties of part-in conformation was further performed. First, the trajectory of the conformation D during the MD simulation was analyzed to validate their structural stability. Fig. S7 shows the typical structure of part-in conformation at initial and final stage of MD simulation. From Fig. S7(a), the contact area between Aβ and Tau in part-in conformation is small in the initial period of MD simulation. At the end of the MD simulation, however, the N-terminal of Aβ and the C-terminal of Tau move closer together, and finally the N-terminal of Aβ insert into the inside of the Tau protein (Fig. S7(b)).

Moreover, solvent accessible surface area (SASA) and the number of water molecules with range of 0.4 nm in the D conformation were calculated during the whole 50 ns (Fig. 5). In Fig. 5(a), the SASA value of Aβ-Tau hybrid decamer gradually decline, ranging from the initial 290 nm^2 falling to 270 nm^2 at the end of MD simulation. Meanwhile, the number of water molecules around Aβ-Tau hybrid decamer within 0.4 nm also decreased from 5200 to 4700 (Fig. 5(b)). These results indicate that the N-terminal of Aβ inserts into the interior of Tau protein, which can make the structure of Aβ-Tau hybrid decamer more compact.

Fig. 6 shows the schematic diagram of the salt-bridge interactions between the residues of the N-terminal of Aβ and them on

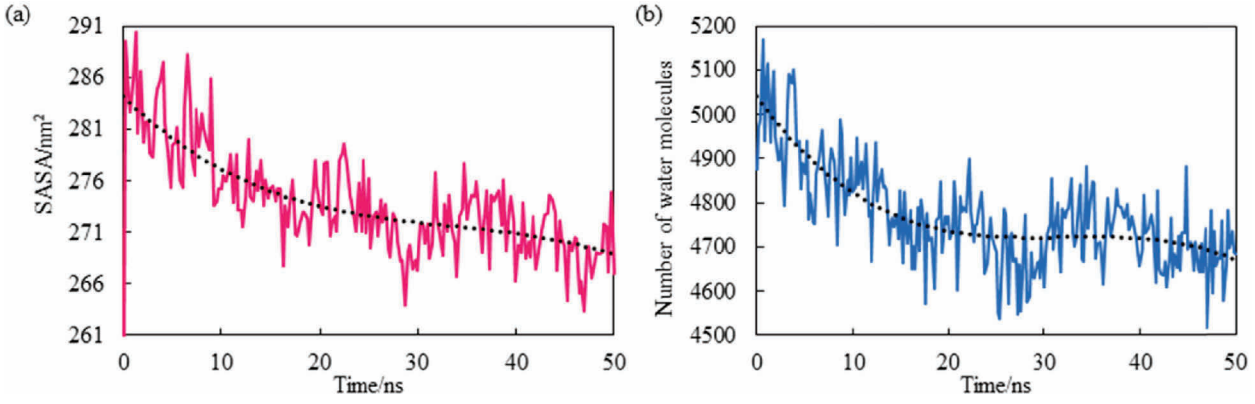

Fig. 5. (a) Values of the solvent accessible surface area (SASA) and (b) the number of water molecules within 0.4 nm of the conformation D (*i.e.*, part-in structure) displayed as a function of simulation time.

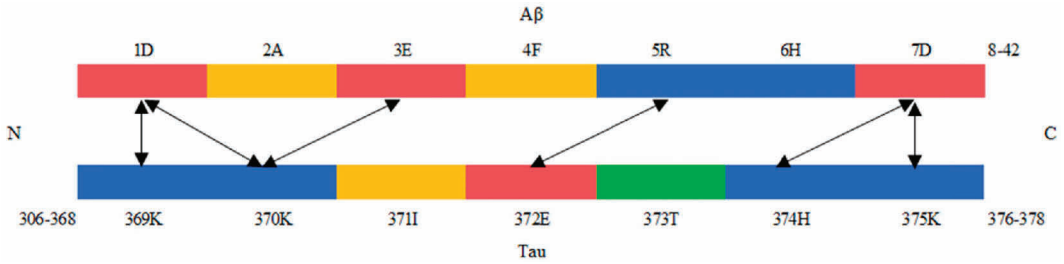

Fig. 6. Residue type in the N-terminal of Aβ and the C-terminal of Tau. The acidic, alkaline, polar, and non-polar amino acids are shown in red, blue, green, and orange, respectively. The possible salt bridge interactions are represented by a two-way black arrow.

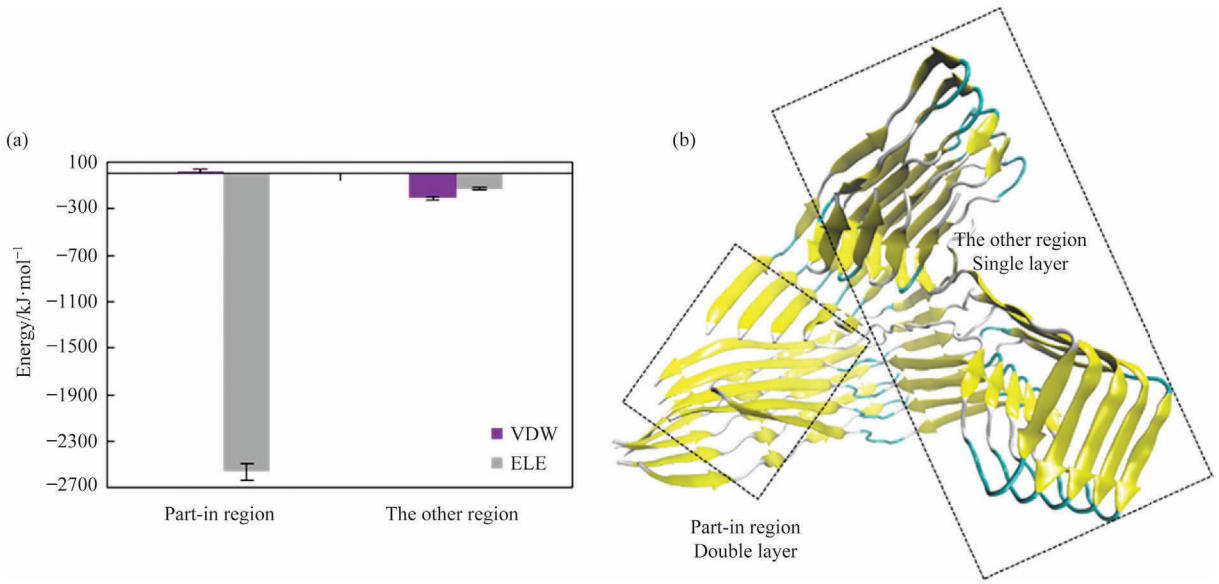

Fig. 7. (a) van der Waals (VDW) and electrostatic (ELE) binding energies between the Aβ pentamer and the Tau pentamer in the part-in region and the other region for the conformation D and (b) the structure of the two regions at the end of the MD simulations.

the C-terminal of Tau. Evidently, six salt bridges formed between Aβ and Tau. It implies that strongest electrostatic interactions exist in the conformation D, consistent with previous energy analysis (Fig. 4(b)).

In addition, the van der Waals and electrostatic interaction analysis was further performed to explore the binding energy between Aβ and Tau (Fig. 7). Herein, N-terminal of Aβ and C-terminal of Tau are defined as the part-in region, and the remaining two regions are viewed as the other region (Fig. 7(b)). And van der Waals and electrostatic energy between the part-in region and the other region were calculated and shown in Fig. 7(a). The results further confirmed that the binding is dominated by the part-in region, while the other region accounts for only about 10%. Moreover, the binding energy in part-in region is dominated by electrostatic interactions although van der Waals interaction is unfavorable in positive. But in the other region, the van der Waals interactions play a dominant role, while the electrostatic interactions have relatively small contribution (Fig. 7(a)).

4. Conclusions

Protein-protein docking and MD simulations were performed to explore the detailed cross-interactions among Aβ-Tau hybrid decamer. Based on the protein-protein docking results, four typical conformations including single layer, block, double layer, and part-in were obtained. Secondary structure analysis of all conformations showed that binding mode of the conformation B (single layer) and C (double layer) can promote the content of β-sheet of Aβ-Tau hybrid decamer. But for the conformation E (double layer), the cross-interactions disrupt the initial β-sheet structure. And then, interaction energies of five conformations were analyzed. It is found that only conformation A has the lowest contact number. While in E conformation, the binding between Aβ and Tau is unfavorable, and the number of contacts is also very little. For conformation D (part-in), the binding energy is the strongest among all the five ones, and the contacts between them are also highly close. Moreover, there are strong hydrogen bonds, salt bridges and hydrophobic interactions in D conformation. Finally, the part-in conformation was further studied in detail. Conformational transition occurs during the MD simulation, and the N-terminal of Aβ partly inserts into the interior of the Tau pentamer. Thus, it led to the increasing of the hydrophobicity of part-in conformation and make its structure closer. Therefore, this work is of great significance for further understanding the mechanism of cross-seeding among amyloid proteins and could help to further understand the molecular mechanism of AD.

Declaration of Competing Interest

The authors declare that they have no known competing financial interests or personal relationships that could have appeared to influence the work reported in this paper.

Acknowledgements

This work was funded by the National Natural Science Foundation of China (21908165 and 21878234) and Regional Innovation System Project (21ZYQCSY00050).

Supplementary Material

Supplementary data to this article can be found online at https://doi.org/10.1016/j.cjche.2022.04.021.

References

[1] F. Bemporad, F. Chiti, Protein misfolded oligomers: Experimental approaches, mechanism of formation, and structure-toxicity relationships, *Chem. Biol.* 19 (3) (2012) 315–327.
[2] H.M. Fan, R.X. Gu, Y.J. Wang, Y.L. Pi, Y.H. Zhang, Q. Xu, D.Q. Wei, Destabilization of Alzheimer's $A\beta_{42}$ protofibrils with a novel drug candidate wgx-50 by molecular dynamics simulations, *J. Phys. Chem. B* 119 (34) (2015) 11196–11202.
[3] M. Margittai, R. Langen, Template-assisted filament growth by parallel stacking of tau, *PNAS* 101 (28) (2004) 10278–10283.
[4] M. von Bergen, S. Barghorn, J. Biernat, E.M. Mandelkow, E. Mandelkow, Tau aggregation is driven by a transition from random coil to beta sheet structure, *Biochim. Biophys. Acta* 1739 (2–3) (2005) 158–166.
[5] S. Jeganathan, M. von Bergen, E.M. Mandelkow, E. Mandelkow, The natively unfolded character of tau and its aggregation to alzheimer-like paired helical filaments, *Biochemistry* 47 (40) (2008) 10526–10539.
[6] R. Morales, L.D. Estrada, R. Diaz-Espinoza, D. Morales-Scheihing, M.C. Jara, J. Castilla, C. Soto, Molecular cross talk between misfolded proteins in animal models of Alzheimer's and prion diseases, *J. Neurosci.* 30 (13) (2010) 4528–4535.
[7] M.I. Ivanova, Y.X. Lin, Y.H. Lee, J. Zheng, A. Ramamoorthy, Biophysical processes underlying cross-seeding in amyloid aggregation and implications in amyloid pathology, *Biophys. Chem.* 269 (2021) 106507.
[8] Y.X. Zhang, M.Z. Zhang, Y.L. Liu, D. Zhang, Y.J. Tang, B.P. Ren, J. Zheng, Dual amyloid cross-seeding reveals steric zipper-facilitated fibrillization and pathological links between protein misfolding diseases, *J. Mater. Chem. B* 9 (15) (2021) 3300–3316.
[9] Y. Wang, G.T. Westermark, The amyloid forming peptides islet amyloid polypeptide and amyloid beta interact at the molecular level, *Int. J. Mol. Sci.* 22 (20) (2021) 11153.
[10] Y. Liang, W.J. Wang, Y. Sun, X.Y. Dong, Insights into the cross-amyloid aggregation of $A\beta_{40}$ and its N-terminal truncated peptide $A\beta_{11-40}$ affected by epigallocatechin gallate, *Chin. J. Chem. Eng.* 45 (2022) 284–293.
[11] M.Z. Zhang, R.D. Hu, H. Chen, Y. Chang, X. Gong, F.F. Liu, J. Zheng, Interfacial interaction and lateral association of cross-seeding assemblies between hIAPP and rIAPP oligomers, *Phys. Chem. Chem. Phys.* 17 (16) (2015) 10373–10382.
[12] K. Konstantoulea, P. Guerreiro, M. Ramakers, N. Louros, L.D. Aubrey, B. Houben, E. Michiels, M. de Vleeschouwer, Y. Lampi, L.F. Ribeiro, J. de Wit, W.F. Xue, J. Schymkowitz, F. Rousseau, Heterotypic Amyloid β interactions facilitate amyloid assembly and modify amyloid structure, *EMBO J.* 41 (2) (2022) e108591.
[13] Y.J. Tang, D. Zhang, Y.L. Liu, Y.X. Zhang, Y.F. Zhou, Y. Chang, B.W. Zheng, A. Xu, J. Zheng, A new strategy to reconcile amyloid cross-seeding and amyloid prevention in a binary system of α-synuclein fragmental peptide and hIAPP, *Protein Sci.* 31 (2) (2022) 485–497.
[14] G.X. Zhang, L.X. Meng, Z.H. Wang, Q.Y. Peng, G.Q. Chen, J. Xiong, Z.T. Zhang, Islet amyloid polypeptide cross-seeds tau and drives the neurofibrillary pathology in Alzheimer's disease, *Mol. Neurodegener.* 17 (2022) 12.
[15] Y. Yang, W. Song, Molecular links between Alzheimer's disease and diabetes mellitus, *Neuroscience* 250 (2013) 140–150.
[16] Y.X. Zhang, Y.J. Tang, D. Zhang, Y.L. Liu, J. He, Y. Chang, J. Zheng, Amyloid cross-seeding between Aβ and hIAPP in relation to the pathogenesis of Alzheimer and type 2 diabetes, *Chin. J. Chem. Eng.* 30 (2021) 225–235.
[17] L. Iaccarino, G. Tammewar, N. Ayakta, S.L. Baker, A. Bejanin, A.L. Boxer, M.L. Gorno-Tempini, M. Janabi, J.H. Kramer, A. Lazaris, S.N. Lockhart, B.L. Miller, Z.A. Miller, J.P. O'Neil, R. Ossenkoppele, H.J. Rosen, D.R. Schonhaut, W.J. Jagust, G.D. Rabinovici, Local and distant relationships between amyloid, tau and neurodegeneration in Alzheimer's disease, *Neuroimage Clin.* 17 (2018) 452–464.
[18] M.A. Busche, S. Wegmann, S. Dujardin, C. Commins, J. Schiantarelli, N. Klickstein, T.V. Kamath, G.A. Carlson, I. Nelken, B.T. Hyman, Tau impairs neural circuits, dominating amyloid-β effects, in Alzheimer models *in vivo*, *Nat. Neurosci.* 22 (1) (2019) 57–64.
[19] M.A. Busche, B.T. Hyman, Synergy between amyloid-β and tau in Alzheimer's disease, *Nat. Neurosci.* 23 (10) (2020) 1183–1193.
[20] B. Vasconcelos, I.C. Stancu, A. Buist, M. Bird, P. Wang, A. Vanoosthuyse, K. Kolen, A. Verheyen, P. Kienlen-Campard, J.N. Octave, P. Baatsen, D. Moechars, I. Dewachter, Heterotypic seeding of Tau fibrillization by pre-aggregated Abeta provides potent seeds for prion-like seeding and propagation of Tau-pathology *in vivo*, *Acta Neuropathol.* 131 (4) (2016) 549–569.
[21] R.E. Bennett, S.L. DeVos, S. Dujardin, B. Corjuc, R. Gor, J. Gonzalez, A.D. Roe, M.P. Frosch, R. Pitstick, G.A. Carlson, B.T. Hyman, Enhanced tau aggregation in the presence of amyloid β, *Am. J. Pathol.* 187 (7) (2017) 1601–1612.
[22] Z.H. He, J.L. Guo, J.D. McBride, S. Narasimhan, H. Kim, L. Changolkar, B. Zhang, R.J. Gathagan, C.Y. Yue, C. Dengler, A. Stieber, M. Nitla, D.A. Coulter, T. Abel, K.R. Brunden, J.Q. Trojanowski, V.M.Y. Lee, Amyloid-β plaques enhance Alzheimer's brain Tau-seeded pathologies by facilitating neuritic plaque Tau aggregation, *Nat. Med.* 24 (1) (2018) 29–38.
[23] J. Lewis, D.W. Dickson, W.L. Lin, L. Chisholm, A. Corral, G. Jones, S.H. Yen, N. Sahara, L. Skipper, D. Yager, C. Eckman, J. Hardy, M. Hutton, E. McGowan, Enhanced neurofibrillary degeneration in transgenic mice expressing mutant tau and APP, *Science* 293 (5534) (2001) 1487–1491.
[24] T. Tripathi, H. Khan, Direct interaction between the β-amyloid core and tau facilitates cross-seeding: A novel target for therapeutic intervention, *Biochemistry* 59 (4) (2020) 341–342.
[25] C. Wallin, Y. Hiruma, S. Warmlander, I. Huvent, J. Jarvet, J.P. Abrahams, A. Graslund, G. Lippens, J. Luo, The neuronal tau protein blocks *in vitro* fibrillation of the amyloid-beta (Abeta) peptide at the oligomeric stage, *J. Am. Chem. Soc.* 140 (26) (2018) 8138–8146.
[26] P.H. Nguyen, A. Ramamoorthy, B.R. Sahoo, J. Zheng, P. Faller, J.E. Straub, L. Dominguez, J.E. Shea, N.V. Dokholyan, A. de Simone, B.Y. Ma, R. Nussinov, S. Najafi, S.T. Ngo, A. Loquet, M. Chiricotto, P. Ganguly, J. McCarty, M.S. Li, C. Hall, Y.M. Wang, Y. Miller, S. Melchionna, B. Habenstein, S. Timr, J.X. Chen, B. Hnath, B. Strodel, R. Kayed, S. Lesné, G.H. Wei, F. Sterpone, A.J. Doig, P. Derreumaux, Amyloid oligomers: A joint experimental/computational perspective on Alzheimer's disease, Parkinson's disease, type II diabetes, and amyotrophic lateral sclerosis, *Chem. Rev.* 121 (4) (2021) 2545–2647.
[27] Y. Miller, B.Y. Ma, R. Nussinov, Synergistic interactions between repeats in Tau protein and Aβ amyloids may be responsible for accelerated aggregation *via* polymorphic states, *Biochemistry* 50 (23) (2011) 5172–5181.
[28] Y. Atsmon-Raz, Y. Miller, Non-amyloid-β component of human α-synuclein oligomers induces formation of new Aβ oligomers: Insight into the mechanisms that link Parkinson's and Alzheimer's diseases, *ACS Chem. Neurosci.* 7 (1) (2016) 46–55.
[29] L. Ciccone, C.H. Shi, D. di Lorenzo, A.C. van Baelen, N. Tonali, The positive side of the Alzheimer's disease amyloid cross-interactions: the case of the $A\beta_{1-42}$ peptide with tau, TTR, CysC, and ApoA1, *Molecules* 25 (10) (2020) 2439.
[30] Y. Atsmon-Raz, Y. Miller, Insight into atomic resolution of the cross-seeding between Tau/Mutated Tau and amyloid-β in neurodegenerative diseases, *Isr. J. Chem.* 55 (6–7) (2015) 628–636.
[31] A.V. Rojas, G.G. Maisuradze, H.A. Scheraga, Dependence of the formation of Tau and Aβ peptide mixed aggregates on the secondary structure of the N-terminal region of aβ, *J. Phys. Chem. B* 122 (28) (2018) 7049–7056.
[32] R.X. Qi, Y. Luo, G.H. Wei, R. Nussinov, B.Y. Ma, Aβ "stretching-and-packing" cross-seeding mechanism can trigger tau protein aggregation, *J. Phys. Chem. Lett.* 6 (16) (2015) 3276–3282.
[33] L. Gremer, D. Schölzel, C. Schenk, E. Reinartz, J. Labahn, R.B.G. Ravelli, M. Tusche, C. Lopez-Iglesias, W. Hoyer, H. Heise, D. Willbold, G.F. Schröder, Fibril structure of amyloid-β_{1-42} by cryo–electron microscopy, *Science* 358 (6359) (2017) 116–119.
[34] A. Fitzpatrick, B. Falcon, S. He, A.G. Murzin, G. Murshudov, H.J. Garringer, R.A. Crowther, B. Ghetti, M. Goedert, S. Scheres, Cryo-EM structures of Tau filaments from Alzheimer's disease, *Nature* 547 (7662) (2017) 185–190.
[35] C. Dominguez, R. Boelens, A.M.J.J. Bonvin, HADDOCK: A protein-protein docking approach based on biochemical or biophysical information, *J. Am. Chem. Soc.* 125 (7) (2003) 1731–1737.
[36] J.C. Gordon, J.B. Myers, T. Folta, V. Shoja, L.S. Heath, A. Onufriev, H++: A server for estimating pKas and adding missing hydrogens to macromolecules, *Nucleic Acids Res.* 33 (Web Server issue) (2005) W368–W371.
[37] R. Anandakrishnan, B. Aguilar, A.V. Onufriev, H++ 3.0: Automating pK prediction and the preparation of biomolecular structures for atomistic molecular modeling and simulations, *Nucleic Acids Res.* 40 (Web Server issue) (2012) W537–W541.
[38] J. Myers, G. Grothaus, S. Narayanan, A. Onufriev, A simple clustering algorithm can be accurate enough for use in calculations of pKs in macromolecules, *Proteins* 63 (4) (2006) 928–938.
[39] X. Daura, K. Gademann, B. Jaun, D. Seebach, W.F. van Gunsteren, A.E. Mark, Peptide folding: When simulation meets experiment, *Angew. Chem. Int. Ed.* 38 (1–2) (1999) 236–240.
[40] D. van der Spoel, E. Lindahl, B. Hess, G. Groenhof, A.E. Mark, H.J.C. Berendsen, GROMACS: Fast, flexible, and free, *J. Comput. Chem.* 26 (16) (2005) 1701–1718.
[41] J. Huang, A.D. MacKerell Jr., CHARMM36 all-atom additive protein force field: Validation based on comparison to NMR data, *J. Comput. Chem.* 34 (25) (2013) 2135–2145.
[42] T. Darden, D. York, L. Pedersen, Particle mesh Ewald: An N·log(N) method for Ewald sums in large systems, *J. Chem. Phys.* 98 (12) (1993) 10089–10092.
[43] L. Verlet, Computer "experiments" on classical fluids. I. Thermodynamical properties of lennard-Jones molecules, *Phys. Rev.* 159 (1) (1967) 98–103.
[44] B. Hess, H. Bekker, H.J.C. Berendsen, J.G.E.M. Fraaije, LINCS: A linear constraint solver for molecular simulations, *J. Comput. Chem.* 18 (12) (1997) 1463–1472.
[45] U. Essmann, L. Perera, M.L. Berkowitz, T. Darden, H. Lee, L.G. Pedersen, A smooth particle mesh Ewald method, *J. Chem. Phys.* 103 (19) (1995) 8577–8593.
[46] M. Parrinello, A. Rahman, Polymorphic transitions in single crystals: A new molecular dynamics method, *J. Appl. Phys.* 52 (12) (1981) 7182–7190.

[47] A. Bondi, Van der waals volumes and radii, *J. Phys. Chem.* 68 (3) (1964) 441–451.
[48] C.Q. Bai, D.D. Lin, Y.X. Mo, J.T. Lei, Y.X. Sun, L.G. Xie, X.J. Yang, G.H. Wei, Influence of fullerenol on hIAPP aggregation: Amyloid inhibition and mechanistic aspects, *Phys. Chem. Chem. Phys.* 21 (7) (2019) 4022–4031.
[49] W. Kabsch, C. Sander, Dictionary of protein secondary structure: Pattern recognition of hydrogen-bonded and geometrical features, *Biopolymers* 22 (12) (1983) 2577–2637.
[50] W. Humphrey, A. Dalke, K. Schulten, VMD: Visual molecular dynamics, *J. Mol. Graph.* 14 (1) (1996) 33–38.
[51] R. Kumari, R. Kumar, O.S.D.D. Consortium, A. Lynn, G_mmpbsa: A GROMACS tool for high-throughput MM-PBSA calculations, *J. Chem. Inf. Model.* 54 (7) (2014) 1951–1962.
[52] S. Linse, Mechanism of amyloid protein aggregation and the role of inhibitors, *Pure Appl. Chem.* 91 (2) (2019) 211–229.
[53] S. Hou, R.X. Gu, D.Q. Wei, Inhibition of β-amyloid channels with a drug candidate wgx-50 revealed by molecular dynamics simulations, *J. Chem. Inf. Model.* 57 (11) (2017) 2811–2821.
[54] M.P. Tang, Z.X. Wang, Y. Zhou, W.J. Xu, S.T. Li, L.Y. Wang, D.Q. Wei, Z.D. Qiao, A novel drug candidate for Alzheimer's disease treatment: Gx-50 derived from Zanthoxylum bungeanum, *J. Alzheimers Dis.* 34 (1) (2013) 203–213.
[55] G. Favrin, A. Irbäck, S. Mohanty, Oligomerization of amyloid $A\beta_{16-22}$ peptides using hydrogen bonds and hydrophobicity forces, *Biophys. J.* 87 (6) (2004) 3657–3664.